NUMERICAL SIMULATION OF THERMO-MECHANICAL BEHAVIOR OF CFRP COMPOSITE LAMINATE SUBJECTED TO LASER PAINT REMOVAL PROCESS USING VARYING BEAM PROFILES IN COMSOL

Rahul Shah [1,†,‡] , Jeremy Laliberte [1,†‡], Hayat EL Fazani [1,†‡], Andrew Fawcett [2,‡], Gianluca Rossi [2,‡]

1 Carleton University, Canada; rahulshah@cmail.carleton.ca
2 Besnovo Inc., Canada; afawcett@besnovo.com
† Carleton University, 1125 Colonel By Drive, Ottawa K1S 5B6, Canada
‡ These authors contributed equally to this work.

Abstract
Removal of paint from Carbon Fiber Reinforced Polymer (CFRP) composites through laser ablation is very promising and environmentally safe process. The typical beam spatial profile of the laser sources used for this process is fundamental mode Gaussian with transverse electromagnetic mode of TEM_{00}. However, there are many other higher order beam modes such as TEM_{01}, TEM_{10} and special beam profiles such as Super-Gaussian (Top-Hat) and Truncated Gaussian that can be used for the process. Potential thermomechanical damage of CFRP composite laminate subjected to laser paint removal process plays a vital role in deciding the efficacy and the accuracy of a particular beam profile. Therefore, analytical studies were first conducted to understand the basic properties of Gaussian beams in terms of their transverse distribution and propagation satisfying the paraxial condition. Secondly, their transformation by simple optics and Diffractive Optical Elements (DOE) to achieve higher orders modes and special beam profiles were also studied. Finally, these studies were then used to model various beam profiles in a commercial finite element package, COMSOL Multiphysics, and to simulate the thermomechanical behavior of CFRP composite laminate illuminated by laser source. Both the Continuous Wave (CW) and Pulsed Laser were simulated. The results were summarized and compared in terms of the temperature distribution in the substrate laminate, penetration depth, and through thickness stresses. It was evident that the Gaussian (TEM_{00}) beam profile has the fastest stabilized time as compared to the Super-Gaussian (Top-Hat) profile but produces higher stresses in the substrate laminate.

1. Introduction

Paints are generally removed from surfaces either by chemicals or abrasives. Although these chemical and abrasive based techniques are effective they do suffer from certain drawbacks. These processes often generate mixed waste and may damage the substrate surface too. Moreover, chemical, or abrasive based methods frequently drive some fraction of the contaminated paint residue deeper into the material, particularly, if the material is porous.

Lasers have been used in wide range of scientific and industrial applications because they offer high energy concentrations, various temporal and spatial distribution and fast processing times. To maximize these advantages, the study of the quality of the processed materials is essential. The

quality of the processed materials is highly influenced by various laser parameters, including laser power, moving speed, beam radius, and beam shape. The optimal processing of laser power and moving speed has been the focus of considerable interest. A growing body of theoretical and experimental work has also explored the spatial structure of the laser beam modes in the areas of modern optics and laser physics [13]. However, one area that has received little quantitative attention is the effects of laser beam spatial distribution or modes on the laser-material interaction process.

While most studies of laser-material interaction modeling have adapted a Gaussian laser beam shape for simplicity [1-4], one often finds several different laser beam shapes, called Transverse Electromagnetic (TEM) modes [12], in a real cavity for the following reasons. First, even in an accurately aligned cavity, some waves travel off-axis as they bounce back and forth, due to the effects of diffraction [10-11]. Second, there is considerable scattering loss that results from scratches on the mirror surface.

In this paper, TEM_{00}, TEM_{01}, TEM_{11}, and Top-hat laser beam shapes are selected. These beam shapes have been chosen due to their popularity as commercially available lasers. The general formula of TEM modes proposed by Enderlein and Pampaloni [13] are modified for all cases to have the same laser power since the definition of the beam radius is different for each case. The four different laser beam modes were used to simulate laser-material interaction.

Moreover, the choice of a particular laser for paint stripping depends on the optical properties of the paint at the irradiation wavelength, paint thickness and on the material from which paint is to be removed. Paint stripping using excimer laser has demonstrated that aluminum and steel substrate retains good surface quality after stripping without getting thermally damaged [15]. However, as the removal of paint per pulse is rather small the processing time is generally longer. Epoxy grey paint stripping with Nd:YAG laser was extensively studied as a function of repetition rate (1 Hz–10 kHz), laser fluence (0.1–5 J/cm^2) and pulse duration (5 ns and 100 ns) [16]. The best paint ablation efficiency of 0.3 mm^3/ (J pulse) was obtained for 10 kHz at 1.5 J/cm^2 for 100 ns pulse. A 1 kW pulsed TEA CO2 laser (pulse energy ~ 3.8 J, repetition rate ~265 Hz) was developed for paint stripping of various metallic and composite aircraft panels [6]. Due to high absorption of CO2 laser radiation in paints and low absorption in the underlying substrate in efficient removal of paint without damaging the substrate

Compared to other lasers, TEA CO2 laser has a distinct advantage in terms of high efficiency, high peak power and higher absorption coefficient [17] for most of the paints. Higher absorption of CO2 laser energy by the paints makes it the ideal choice for paint stripping and was the choice for this research.

2. Mathematical Model of Various Laser Beam Modes

2.1. Fundamental Gaussian Beam Mode (TEM_{00})

By solving the Paraxial Helmholtz equation [33], the complex amplitude U(r) of the Gaussian Beam is expressed as:

$$U(r) = A_0 \frac{W_0}{W(Z)} exp\left[-\frac{\rho^2}{W(Z)^2}\right] exp\left[-jkz - jk\frac{\rho^2}{2R(Z)} + j\xi(Z)\right] \quad (2.1)$$

Where,

$$W(Z) = W_0\sqrt{1+\left(\frac{Z}{Z_0}\right)^2} = \text{Beam waist radius at distance "Z".}$$

$$R(Z) = Z\left[1+\left(\frac{Z_0}{Z}\right)^2\right] = \text{Raileigh range}$$

$$W_0 = \sqrt{\frac{\lambda Z_0}{\pi}} = \text{Beam waist radius}$$

$$\xi(Z) = \tan^{-1}\frac{Z}{Z_0}$$

The optical Intensity I(r) = U(r)^2 of the Gaussian Beam is a function of the axial and radial positions, Z and $\rho = \sqrt{x2 + y2}$, respectively and it is expressed as:

$$I(\rho, z) = I_0\left[\frac{W0}{W(Z)}\right]^2 exp^{\left[-\frac{2\rho^2}{W(Z)^2}\right]}$$

The optical intensity I(r) of a Gaussian Beam in terms of the laser power (P) is expressed as:

$$I(\rho, z) = \frac{2P}{\pi W(Z)^2} exp^{\left[-\frac{2\rho^2}{W(Z)^2}\right]} \tag{2.3}$$

Figure-1-(a) shows the normalised Gaussian Beam intensity as a function of radial distance "ρ" at different axial distances "Z". Equation (2.3) is the mathematical expression for TEM_{00} Gaussian Beam profile. Figure-1-(a) shows the Gaussian Beam profile generated in COMSOL based on Equation (2.3).

2.2. Higher Order Gaussian Beam Mode (TEM_{01})

The Gaussian beam is not the only beam-like solution of a Paraxial Helmholtz equation [12-13]. Of particular interest are solutions that exhibit non-Gaussian intensity distributions but share the wave fronts of the Gaussian Beam [33]. These solutions are called the Hermite Polynomial or Hermite-Gaussian functions and is expressed as:

$$U_{l,m}(x, y, z) = \left|A_{l,m}\right|\left[\frac{W_0}{W(Z)}\right] G_l\left[\frac{\sqrt{2}X}{W(Z)}\right] G_m\left[\frac{\sqrt{2}Y}{W(Z)}\right] exp^{\left[-jkz-jk\frac{X^2+Y^2}{2R(Z)}+j(l+m+1)\xi(Z)\right]} \tag{2.4}$$

Where,

$$G_l(u) = H_l(u)\, exp^{\left(-\frac{u^2}{2}\right)}, l = 0, 1, 2, \ldots$$

Equation (2.4) is known as the Hermite-Gaussian function of order "l" and $A_{l,m}$ is a constant. Since $H_0(u) = 1$, the Hermite-Gaussian function of order "0" is simply the Gaussian function. Continuing to higher order, $G_1(u) = 2u*\exp(-u^2/2)$ is an odd function, $G_2(u) = (4u^2 - 2)*\exp(-u^2/2)$ is even, $G_3(u) = (8u^3 - 12u)*\exp(-u^2/2)$ is odd and so on. These functions are displayed schematically in Figure-1(b) below:

The optical intensity I(r) of $HG_{l,m}$ order Hermite-Gaussian Beam is expressed as:

$$I_{l,m}(x, y, z) = \left|A_{l,m}\right|^2\left[\frac{W_0}{W(Z)}\right]^2 {G_l}^2\left[\frac{\sqrt{2}X}{W(Z)}\right] {G_m}^2\left[\frac{\sqrt{2}Y}{W(Z)}\right]$$

(2.5)

For $HG_{01} = TEM_{01}$; For l = 0, $G_l = G_0(u) = \exp(-u^2/2)$ and for m =1, $G_m = G_1(u) = 2v*\exp(-v^2/2)$ and for Z = 0; $W(Z) = W_0$. Hence, equation (2.5) will be expressed as:

$$I_{l,m}(x, y, z) = \frac{2P}{\pi W(Z)^2}\left[\frac{\sqrt{2X}}{W(Z)}\right]\left(exp^{\left[-\frac{X^2}{2}\right]}\right)^2\left[\frac{4Y^2}{W(z)^2}\right]\left(exp^{\left[-\frac{Y^2}{W(z)^2}\right]}\right)^2 \quad (2.6)$$

Equation (2.6) is the mathematical expression for TEM_{01} Beam profile. Figure-1(b) shows the TEM_{01} Higher-order Gaussian Beam profile generated in COMSOL based on equation (2.6):

2.3. Higher Order Gaussian Beam Mode (TEM_{11})

For $HG_{11} = TEM_{11}$; For l = 1, $G_l = G_1(u) = 2u*\exp(-u^2/2)$; for m =1, $G_m = G_1(u) = 2v*\exp(-v^2/2)$. Hence, equation (2.5) will be expressed as:

$$I_{l,m}(x, y, z) = \frac{P}{2\pi W(Z)^2}\left[\frac{8X^2}{W(Z)^2}\right] exp^{\left(-\frac{2X^2}{W(Z)^2}\right)}\left[\frac{8Y^2}{W(Z)^2}\right] exp^{\left(-\frac{2Y^2}{W(Z)^2}\right)} \quad (2.7)$$

Equation (2.7) is the mathematical expression for TEM_{11} Beam profile. Figure-1(c) illustrates the dependence of the intensity on the normalized transverse distances u =$\frac{\sqrt{2x}}{W(Z)}$ and v = $\frac{\sqrt{2y}}{W(Z)}$ for several values of "l" and "m". Figure-1(c) shows the TEM_{11} Higher-order Gaussian Beam profile generated in COMSOL based on equation (2.7):

2.4. Top-Hat or Flat-Top Beam (Super-Gaussian)

The heat generated by a super-Gaussian profile (i.e., a smoothed flat-top profile) of transverse optical intensity of order "n" [1] can be given as:

$$Q(r) = Q_0 \exp\left[-2\left(\frac{r}{w_0}\right)^n\right] \quad (2.8)$$

Where, Q_0 is the peak intensity, w_0 is the beam radius over the incident surface, and r is the radial distance from the propagation axis. A conventional Gaussian profile results from a super-Gaussian one of order two; the higher the order [34], the steeper the edges of the profile. A super-Gaussian intensity profile of "order 20" was implemented [35] as shown in Figure-1(d), based on actual data acquisition via beam profiler [55]. Under this assumption and for "P" denoting the operating power, the peak intensity in Equation (2.8) approaches:

$$Q_0 = \frac{P}{\pi w_0^2}$$

With x_0 and y_0 being the coordinates of the starting point of the beam path, a heat source was implemented in a Cartesian coordinate system, hence Equation (2.8) yielding:

$$Q(x,y) = \frac{P}{\pi w_0^2} \exp\left\{ -\frac{2\left[(x-x_0)^{20}+(y-y_0)^{20}\right]}{w_0^{20}} \right\}$$

(2.9)

Equation (2.9) is the mathematical expression for Top-Hat Beam profile. Figure-1(d) shows the Top-Hat (Super-Gaussian) Beam profile generated in COMSOL based on equation (2.9):

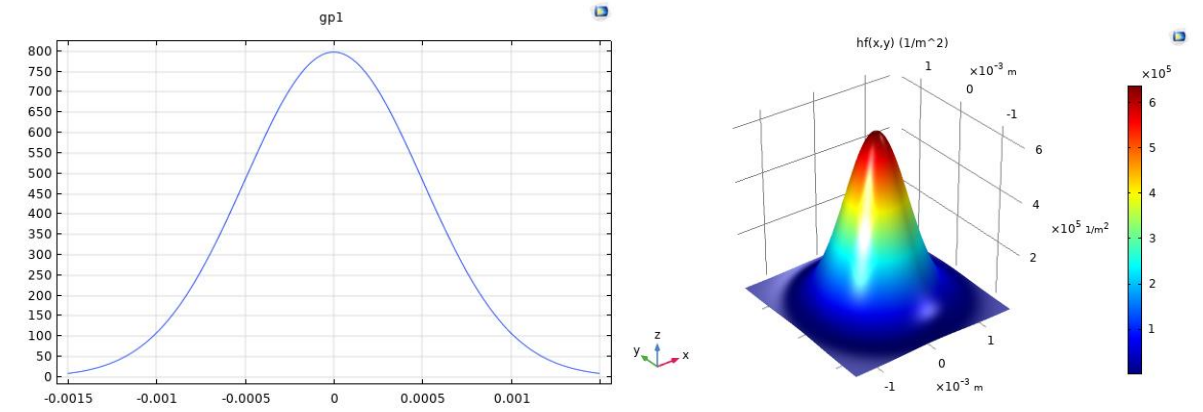

(a)

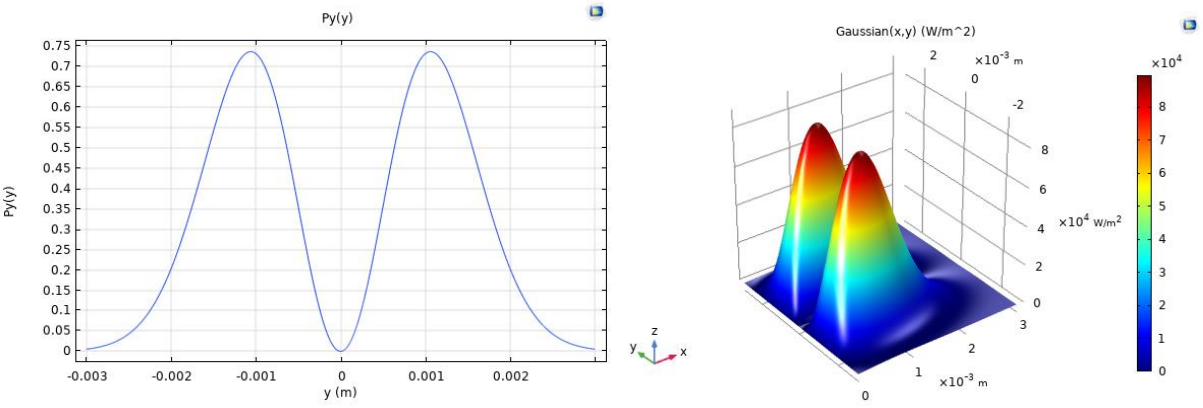

(b)

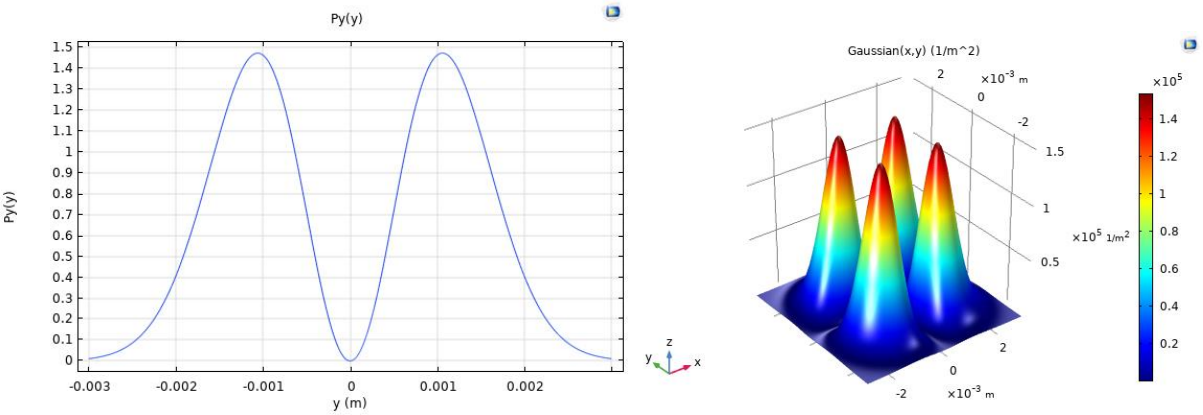

(c)

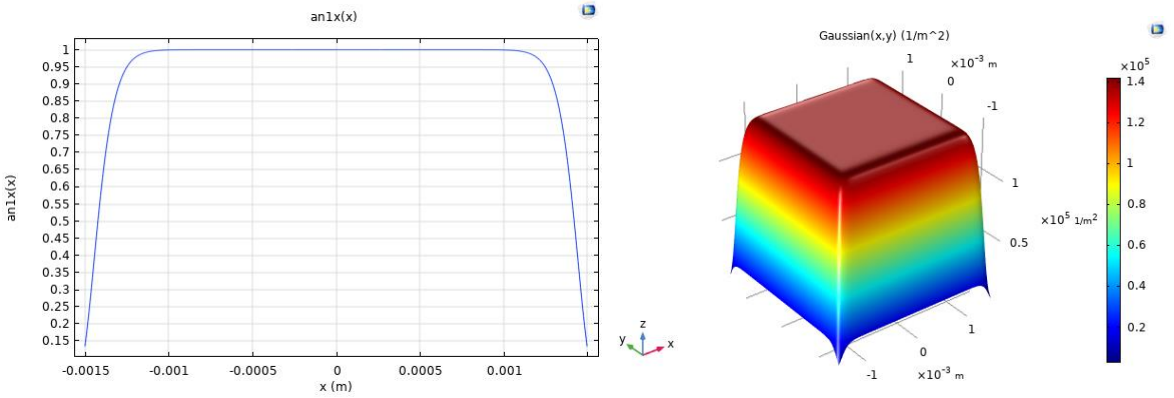

Figure-1 Beam profile in COMSOL for Beam waist radius W0 = 1.5mm, (a) TEM_{00} Gaussian Beam (b) TEM_{01} Gaussian Beam (c) TEM_{11} Gaussian Beam (d) Top-Hat Super-Gaussian Beam

3. Mathematical Model of Heat Transfer in Substrate Material

Heat generated by a laser beam at the paint surface is dissipated by conduction, convection, and radiation [2]. The heat transport equation can be defined as:

$$\rho c \frac{\partial T}{\partial t} = \nabla \cdot (k \nabla T) + \alpha Q \tag{3.1}$$

Where, ρ is the density, C is the heat capacity, T is the temperature, K is the thermal conductivity, α is the absorption coefficient and Q is the laser heat generation. If we include the terms for the heat dissipated by convection and radiation, equation (4.1) takes the form as below:

$$\rho c \frac{\partial T}{\partial t} - \nabla . (K \nabla T) = Q + \frac{h_{trans}}{dA} (T_{ext} - T) + \varepsilon \sigma ({T_{amb}}^4 - T^4) \tag{3.2}$$

Where, h_{trans} is the heat transfer coefficient, ε is the emissivity, σ is the Stefan-Bolzman constant. The described model is applicable if there is no phase transition and other substantial surface changes i.e. for temperature profile below the melting point. At present we are only interested in thermo-mechanical behavior of laser heating of a substrate with paint material. Therefore, we shall apply the above assumptions and use the heat transfer equation in our numerical simulation.

3.1. Beer-Lambert Law for Energy Absorption by Paint Layer

The process of a plate of homogeneous and isotropic material absorbing a monochromatic and parallel laser beam of incident power density I_0 can be described by the Beer-Lambert law [8, 62]:

$$I = I_0 e^{-\propto Z} \tag{3.3}$$

where I is the depth dependent laser intensity and I_0 is the surface laser intensity of different laser beam modes as defined in section-2 and α is the spectral linear absorption coefficient (cm^{-1}) of the material at laser wavelength.

4. Material Properties for Numerical Simulation

4.1. Epoxy Paint

In the present paper, Epoxy paint is used as it is widely used in industry because of its excellent chemical and water resistance and good adhesion to CFRP laminate. Moreover, it is a standard paint material whose mechanical and thermal properties are well documented in the literature [22-25] and tabulated here in Table 1. FTIR spectroscopy of epoxy paint was carried out [64] to measure the absorption coefficient (α) and the value comes out to be $14.9x10^2$ (cm^{-1}).

Table 1 Thermal Properties of Epoxy Paint

Property	**Value**	**Unit**
Specific Heat (Cp)	1180	J/(Kg*K)
Thermal Conductivity (K)	0.2	W/(m*K)
Coefficient of Thermal Expansion (α1)	$55x10^{-6}$	[1/K]
Density (ρ)	1800	Kg/m^3
Absorption Coefficient (α) at 10.6μm Wavelength	$14.9x10^2$	(cm^{-1})

4.2. Carbon Fiber Reinforced Composite Plastic (CFRP) Substrate Laminate

As per the SAE4872A standard [20], the recommended material properties for using CFRP composite for an aircraft structure is specified as BMS 8-256, Type IV, Class 2, 3K-70-PW (Ply Thickness: 8.5 mil +/- 0.8 mil) – 350F Cure CFRP. According to this recommendation, we have used CYCOM® 997 Epoxy Resin system and the properties [14] of it are listed in Table 2. The mechanical properties [15] of a single ply laminate made with Unidirectional Prepreg Tape of CYCOM® Epoxy Resin system are tabulated in Table 3. The temperature dependent thermal properties [21-23] of a single ply CFRP laminate with Unidirectional Prepreg Tape of CYCOM® Epoxy Resin system are tabulated in Table 5. The coefficient of thermal expansion for a single ply unidirectional laminate are obtained by rule of mixture. Laminate sequence used for the CFRP composite panel is $[0, 90,4\ 5, -45]_{2S}$ with total thickness of the laminate as 2.2 mm.

Table 2 Mechanical Properties of CYCOM® Epoxy Resin Matrix

Property	**Value**	**Unit**
Elastic Modulus (E11)	4.14	GPa
Elastic Modulus (E22)	4.14	GPa
Shear Modulus (G12)	1.172	GPa
Poison's Ratio	0.35	-
Density (rho)	1265	Kg/m^3

Table 3 Mechanical Properties of a Single Unidirectional CFRP Laminate

Particular	**Value**	**Unit**
Longitudinal Young's Modulus (Ec,x)	131	GPa
Transverse Young's Modulus (Ec,y)	4.0	GPa
Shear Modulus (Ec,s)	4.8	GPa
Major Poisson's Ratio (Vc,x)	0.28	-
Minor Poisson's Ratio (Vc,y)	0.28	-
Fibre Volume Fraction, V_F	60%	-
Cured thickness – Single Ply Laminate	0.1375	mm

Table 4 Thermal Properties of Single Ply Unidirectional CFRP Laminate for Static Analysis

Particular	**Value**	**Unit**
Fibre Volume Fraction, V_F	0.6	-
Matrix Volume Fraction, Vm	0.4	-
Fibre Young Modulus in Fibre Direction, E1f	230	GPa
Matrix Young Modulus, Em	4.14	GPa
Fibre Poisson's Ratio, $V_{12}f$	0.2	-
Matrix Poisson's Ratio Vm	0.35	-
Fibre Thermal Expansion Coefficient in Fibre Direction, α1f	-0.6E6	[1/K]
Fibre Thermal Expansion Coefficient Perpendicular to Fibre Direction, α2f	8.5E-6	[1/K]
Thermal Expansion Coefficient in Fibre Direction, α11	3.72E-8	[1/K]
Thermal Expansion Coefficient Perpendicular to Fibre Direction, α22, α33	3.47E-5	[1/K]
Laminate Thermal Conductivity, Fiber Direction, K1	6.2	W/(m*K)
Laminate Thermal Conductivity, Perpendicular to Fiber Direction, K2	0.5	W/(m*K)
Laminate Specific Heat (Cp)	465	J/(Kg*K)
Density (ρ)	1600	Kg/m^3

Table 5 Temperature Dependent Thermal Properties of Single Ply Unidirectional CFRP Laminate

T(K)	**Cp J/(Kg*K)**	**K1 W/(m*K) Fiber Direction**	**K2 W/(m*K) Perp. To Fiber Direction**	**α1 [1/K]x10^{-7}**	**α2 [1/K]x10^{-5}**
300	850	7.0	0.80	-3.0	3.2
350	930	8.0	0.85	-7.0	4.2
400	1100	8.5	0.90	-7.5	6.5
500	1300	9.0	0.93	-10.0	6.8

4.3. Properties of TEA CO_2 Laser for Numerical Simulation

Compared to other lasers, TEA CO2 laser has a distinct advantage in terms of high efficiency, high peak power and higher absorption coefficient [62] for most of the paints. Higher absorption of CO2 laser by the paints makes it the ideal choice for paint stripping. Therefore, in this paper the TEA CO2 laser has been used for the numerical simulation and the properties of which are listed in Table 6. Figure-2 shows the pulse generation using analytical function with periodic excitation in COMSOL. The simulation is run for total 1 millisecond.

Table 6 Properties of TEA CO2 Laser

Description	**Value**	**Unit**
Wavelength (λ)	10.6	μm
Laser Power (W)	800	Watt
Pulsed Width	200	Microseconds (μs)
Beam Waist Radius (W_0)	1.5	mm

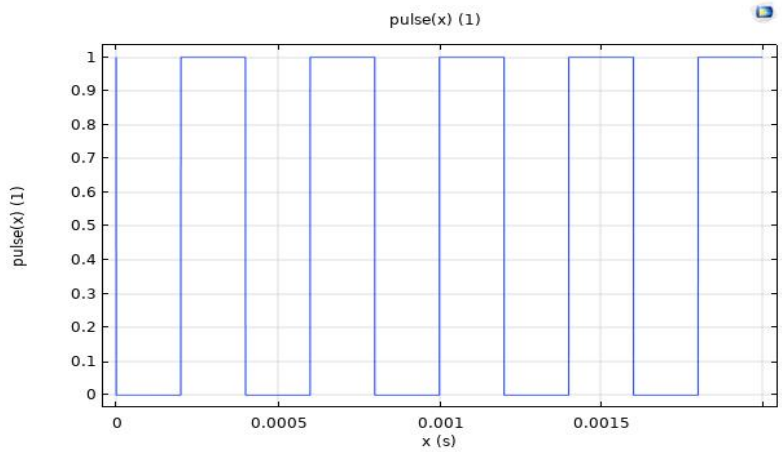

Figure-2 Analytic function in COMSOL to depict pulsed laser with pulse width of 200 μs

5. Simulation in COMSOL

COMSOL Multiphysics is used for Modeling of laser heating and subsequent thermo-mechanical behaviour of a substrate with paint material. COMSOL has a unique capability to model very thin layered material via "Layered Shell" interface. The "Heat Transfer in Layered Shell" interface is used for generating laser heat source and simulating heat transfer as per Equation (3.2). A two-dimensional square plate with dimension: 250 mm (L) x 250 mm (W) is modeled. The thickness of the plate is defined by the CFRP laminate with total 16 numbers of ply plus one layer of Epoxy paint (250 μm thickness) using the "Layered Shell" interface in COMSOL. The following boundary condition adopted for heat transfer in COMSOL: Inward heat flux applied at the top surface, heat dissipated by convection and radiation at the top surface and the edges are insulated. Layered cross section preview for CFRP composite with Epoxy paint layer is shown in Figure-3 and the layer stack preview is shown in Figure-4. The Multiphysics capacity of COMSOL is used for running multiple physics together. Here we run the model for coupled "Heat Transfer in Layered Shell" and "Structural Mechanics" physics to get the deformation, stresses, and temperature distribution.

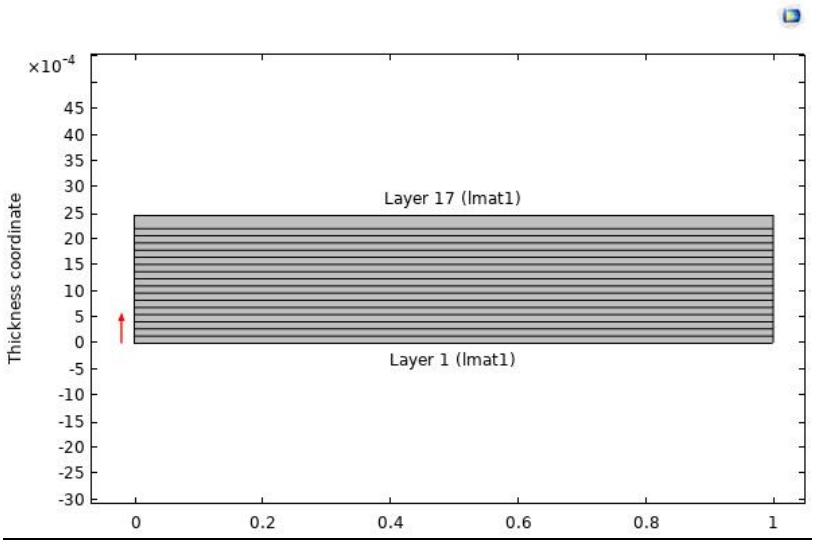

Figure-3 Layer Cross Section Preview for Laminate Sequence $[0, 90, 45, -45]_{2s}$ = 16 layers for CFRP Composite Panel with Epoxy Paint

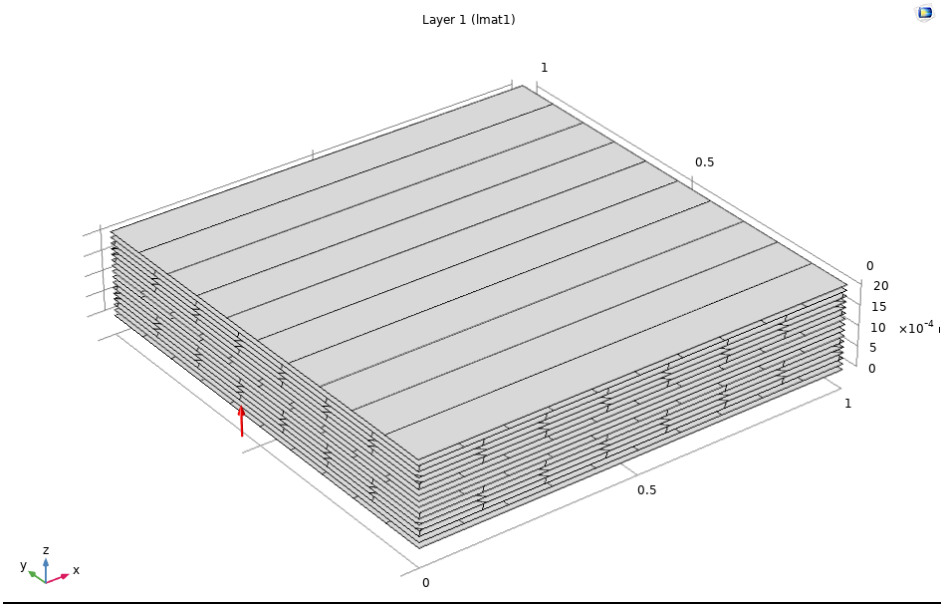

Figure-4 Layer Stack Preview for Laminate Sequence $[0, 90, 45, -45]_{2s}$ = 16 layers for CFRP Composite Panel with Epoxy Paint

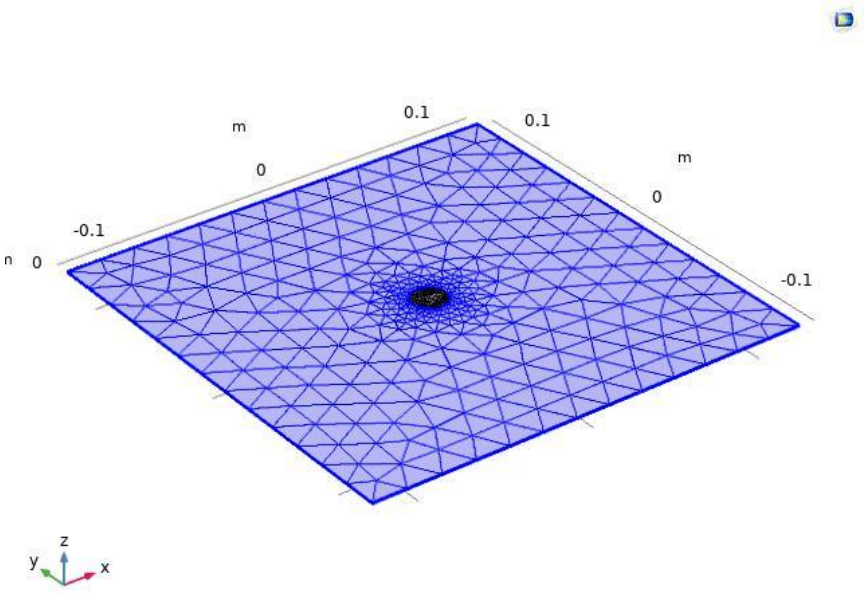

Figure-5 Meshed geometry of CFRP composite panel with Epoxy paint

6. Results and Discussion

The simulation is run for both Stationary and Transient (Time-Dependent) analysis. The results of the simulation are summarized in as shown in the section 6.1 and 6.2 in terms of the temperature distribution, von-mises stresses and through thickness stresses in the substrate material.

6.1. Stationary Analysis

The stationary analysis is performed with Gaussian TEM_{00} and Top-Hat beam profiles with the laser power intensity of 60W. The results are summarized in terms of the temperature and von-mises stress distribution in the substrate laminate as shown in Figure-6 and Figure-7.

6.2. Stationary Analysis

The transient (time-dependent) analysis is performed for total of 10 milliseconds with Gaussian TEM_{00} and Top-Hat beam profiles with the laser power intensity of 800W and Pulse width of 200 microseconds. The results are summarized in terms of the temperature distribution in the substrate laminate as shown in Figure-8 and Figure-9. The von-mises stress distribution in the substrate laminate was also compared.

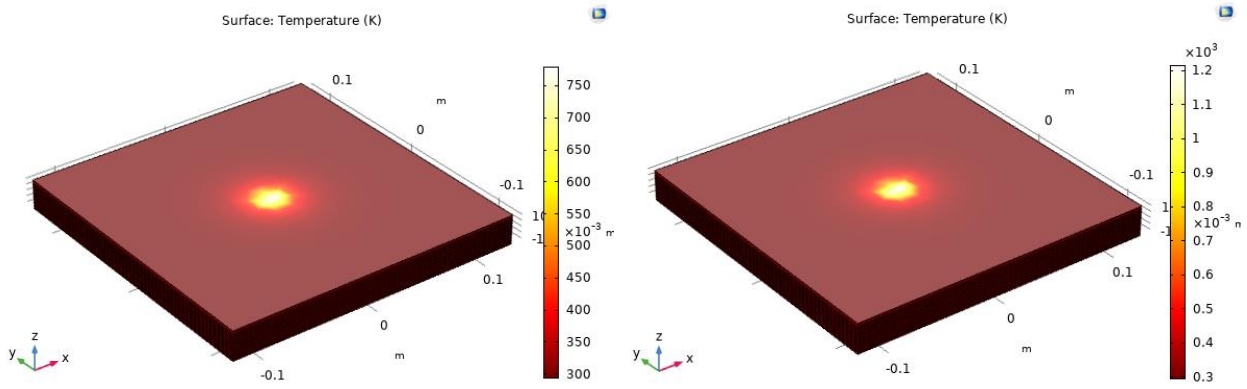

(a) (b)

Figure-6 Temperature distribution for stationary analysis (a) Gaussian TEM_{00} and (b) Top- Hat Beam Profiles

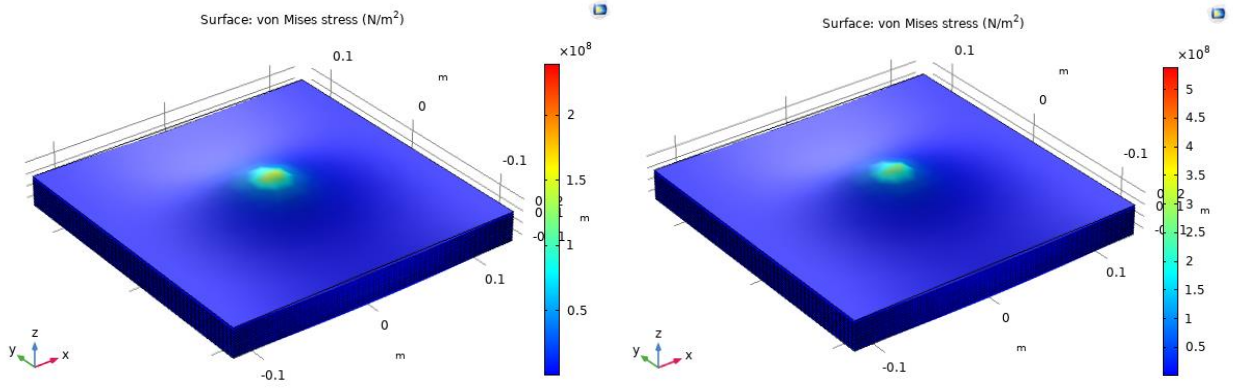

(a) (b)

Figure-7 Von-Mises stress distribution for stationary analysis (a) Gaussian TEM_{00} and (b) Top- Hat Beam Profiles

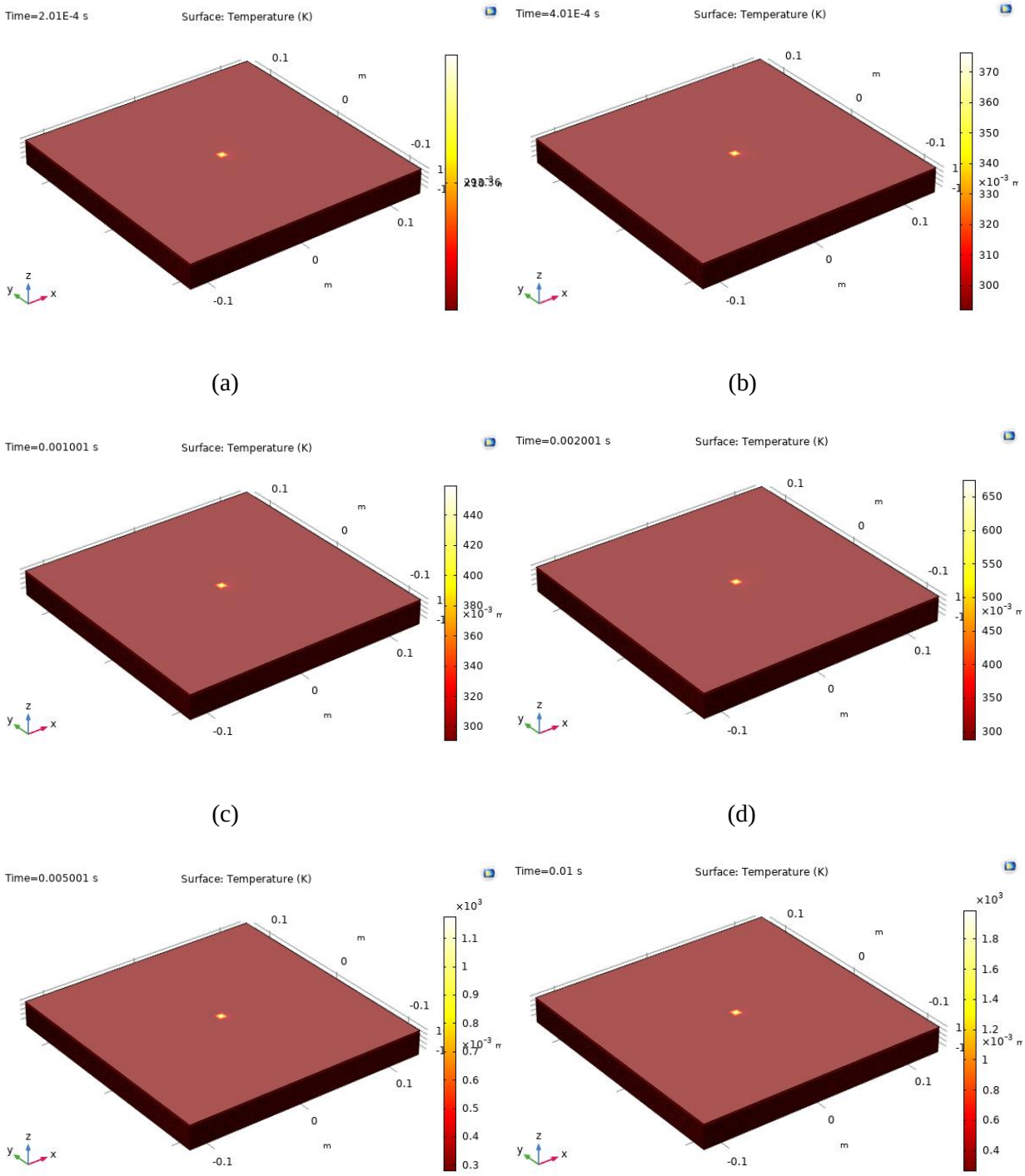

Figure-8 Pulsed laser simulation with Gaussian (TEM_{00}) beam profile: Temperature distribution at (a) 200 μs (b) 400 μs (c) 1 Millisecond (d) 2 Milliseconds (e) 5 Milliseconds (f) 10 Milliseconds

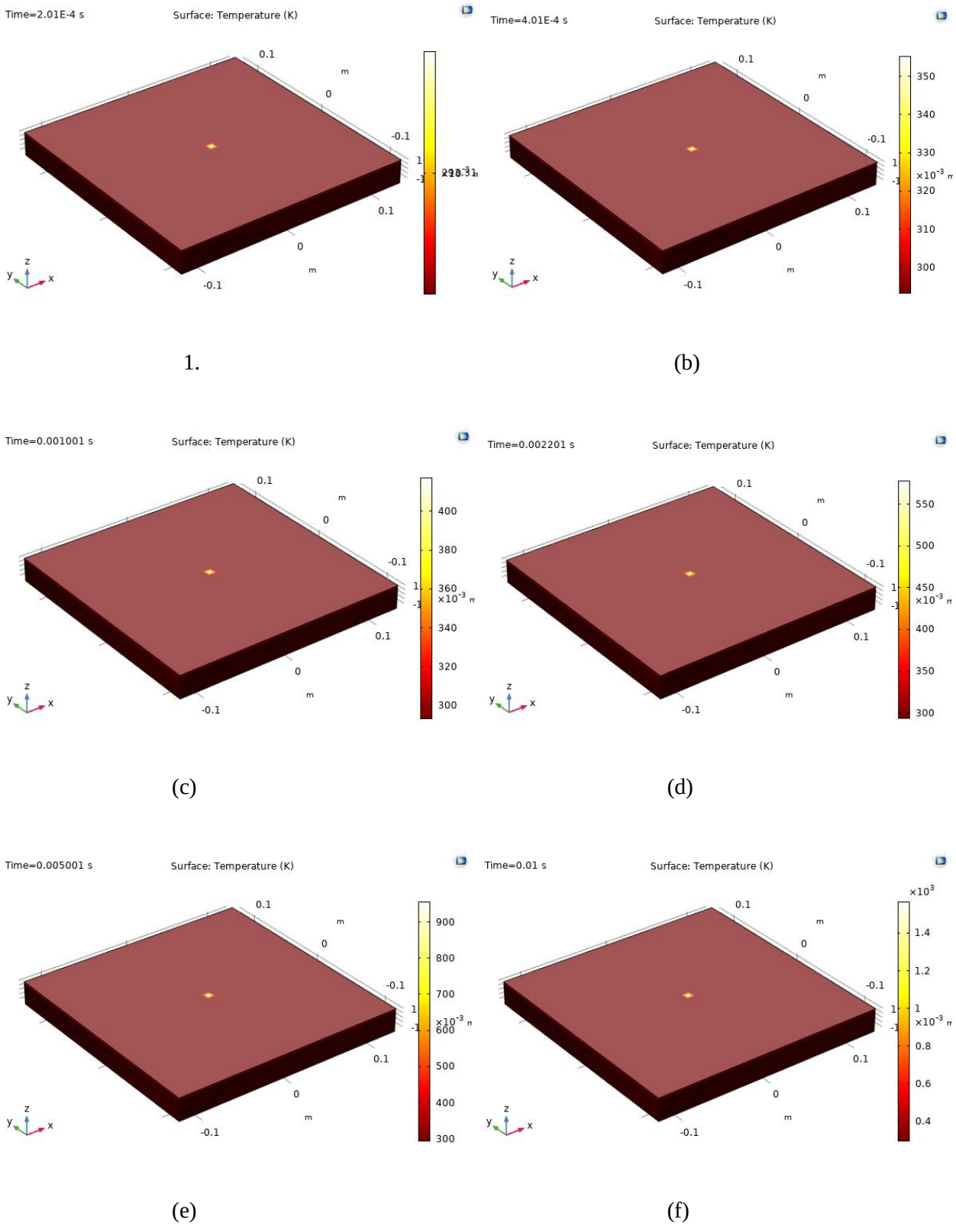

Figure-9 Pulsed laser simulation with Top-Hat beam profile: Temperature distribution at (a) 200 μs (b) 400 μs (c) 1 Millisecond (d) 2 Milliseconds (e) 5 Milliseconds (f) 10 Milliseconds

7. Future Work

The next step in this work is to compare the depth of penetration as a function of number of pulses and laser fluence. Furthermore, the analysis of Heat Affected Zone (HAZ) and residual stresses generated will be carried out and will be compared with different beam profiles used. A two-dimensional thickness model will also be generated considering the phase change/transition of the paint from solid to gaseous state due to the laser heat source and complete material removal process will be simulated.

8. Conclusion

The numerical modeling approach developed in this research was shown to produce good results and following conclusion can be made:

1. From the stationary analysis results, it is evident that the temperature distribution in the substrate laminate is higher in case of Top-Hat beam profile as compared to the Gaussian (TEM_{00}) beam profile. However, the Top-Hat beam profile generate higher stresses in the substrate laminate than the Gaussian (TEM_{00}) beam profile.

2. From the results of transient (time-dependent analysis), it was observed that for the Gaussian (TEM_{00}) beam profile, it takes 1.6 milliseconds to reach the substrate temperature of 550K and 4.2 milliseconds for 1000K. Whereas, for the Top-Hat beam profile, it takes 2 milliseconds to reach the substrate temperature of 550K and 5 milliseconds for 1000K. So, it can be concluded the Gaussian (TEM_{00}) beam profile has a smaller stabilized time as compared to the Top-Hat beam profile for the same laser power intensity.

3. From the results of transient (time-dependent analysis), it was observed that the stress distribution in the substrate laminate is higher with Gaussian (TEM_{00}) beam profile than the Top-Hat beam profile.

References

[1] Rüdiger Paschotta, *Encyclopedia of Laser Physics and Technology*, vol. A-M. Willey-VCH, 2009.

[2] E. Kundakcioglu, I. Lazoglu, and S. Rawal, "Transient thermal modeling of laser-based additive manufacturing for 3D freeform structures," *International Journal of Advanced Manufacturing Technology*, vol. 85, no. 1–4, 2016, doi: 10.1007/s00170-015-7932-2.

[3] J. H. Cho and S. J. Na, "Implementation of real-time multiple reflection and Fresnel absorption of laser beam in keyhole," *Journal of Physics D: Applied Physics*, vol. 39, no. 24, 2006, doi: 10.1088/0022-3727/39/24/039.

[4] R. Rai, G. G. Roy, and T. Debroy, "A computationally efficient model of convective heat transfer and solidification characteristics during keyhole mode laser welding," *Journal of Applied Physics*, vol. 101, no. 5, 2007, doi: 10.1063/1.2537587.

[5] H. Ki, P. S. Mohanty, and J. Mazumder, "Modeling of laser keyhole welding: Part II. Simulation of keyhole evolution, velocity, temperature profile, and experimental verification," *Metallurgical and Materials Transactions A: Physical Metallurgy and Materials Science*, vol. 33, no. 6, 2002, doi: 10.1007/s11661-002-0191-5.

[6] H. Ki, P. S. Mohanty, and J. Mazumder, "Modeling of laser keyhole welding: Part I. Mathematical modeling, numerical methodology, role of recoil pressure, multiple reflections, and free surface evolution," *Metallurgical and Materials Transactions A: Physical Metallurgy and Materials Science*, vol. 33, no. 6, 2002, doi: 10.1007/s11661-002-0190-6.

[7] M. Emonts, K. Fischer, S. Schmitt, and R. L. Schares, "Modelling of indirect laser-induced

thin-film ablation of epoxy for local exposing of carbon fibers," in *Physics Procedia*, 2016, vol. 83. doi: 10.1016/j.phpro.2016.08.142.
[8] Sandeep Kumar Ravi Kumar, "Experimental studies and simulation of laser ablation of high-density polyethylene films," 2020.
[9] D. Yuan and S. Das, "Experimental and theoretical analysis of direct-write laser micromachining of polymethyl methacrylate by CO2 laser ablation," *Journal of Applied Physics*, vol. 101, no. 2, Jan. 2007, doi: 10.1063/1.2409621.
[10] P. G. Berrie and F. N. Birkett, "The drilling and cutting of polymethyl methacrylate (Perspex) by CO2 laser," *Optics and Lasers in Engineering*, vol. 1, no. 2, Oct. 1980, doi: 10.1016/0143-8166(80)90003-2.
[11] N. C. Nayak, Y. C. Lam, C. Y. Yue, and A. T. Sinha, "CO2-laser micromachining of PMMA: The effect of polymer molecular weight," *Journal of Micromechanics and Microengineering*, vol. 18, no. 9, 2008, doi: 10.1088/0960-1317/18/9/095020.
[12] J Wilson; J F B Hawkes, *Lasers, Principle and Applications*. New York: Prentice Hall, 1987.
[13] R. , O. P. J. Crafer, *Laser Processing in Manufacturing*, 1st ed. Springer, 1993.
[14] Koichi Shimoda, *Introduction to Laser Physics*, 2nd ed. Springer, 1986.
[15] E. I. Ugwu, J. E. Ekpe, E. Nnaji, and E. H. Uguru, "Theoretical Study of Electromagnetic Wave Propagation: Gaussian Bean Method," *Applied Mathematics*, vol. 04, no. 10, 2013, doi: 10.4236/am.2013.410198.
[16] "CYCOM 997 Epoxy Resin," *Solvay*.
[17] J. A. Esfahani and A. C. M. Sousa, "Ignition of epoxy by a high radiation source. A numerical study," *International Journal of Thermal Sciences*, vol. 38, no. 4, 1999, doi: 10.1016/S1290-0729(99)80097-0.
[18] F. J. Prinsloo, S. P. van Heerden, E. Ronander, and L. R. Botha, "Efficient TEA CO 2 -laser-based coating removal system," Sep. 2006. doi: 10.1117/12.739109.
[19] F. Brygo, C. Dutouquet, F. le Guern, R. Oltra, A. Semerok, and J. M. Weulersse, "Laser fluence, repetition rate and pulse duration effects on paint ablation," *Applied Surface Science*, vol. 252, no. 6, 2006, doi: 10.1016/j.apsusc.2005.02.143.
[20] L. M. Galantucci, A. Gravina, G. Chita, and M. Cinquepalmi, "An experimental study of paint-stripping using an excimer laser," *Polymers and Polymer Composites*, vol. 5, no. 2, 1997.
[21] A. Forbes, N. C. du Preez, V. Belyi, and L. R. Botha, "Paint stripping with high power flattened Gaussian beams," in *Laser Beam Shaping X*, 2009, vol. 7430. doi: 10.1117/12.829173.
[22] SAE Aerospace, "Paint Stripping of Commercial Aircraft - Evaluation of Materials and Processes," *SAE Aerospace*, 1998.
[23] O. Pirgon, G. H. Wostenholm, and B. Yates, "Thermal expansion at elevated temperatures IV. Carbon-fibre composites," *Journal of Physics D: Applied Physics*, vol. 6, no. 3, 1973, doi: 10.1088/0022-3727/6/3/304.
[24] R. Joven, R. Das, A. Ahmed, P. Roozbehjavan, and B. Minaie, "Thermal properties of carbon fiber-epoxy composites with different fabric weaves," 2012.
[25] E. P. Scott and J. v. Beck, "Estimation of Thermal Properties in Epoxy Matrix/Carbon Fiber Composite Materials," *Journal of Composite Materials*, vol. 26, no. 1, 1992, doi: 10.1177/002199839202600109.
[26] A. Kovačević, M. Srećković, R. Gospavić, S. Ristić, and P. Jovanić, "Laser-PMMA interaction and mechanical stresses," in *Acta Physica Polonica A*, 2007, vol. 112, no. 5. doi: 10.12693/APhysPolA.112.981.
[27] D. Savastru, R. Savastru, I. Lancranjan, S. Miclos, and C. Opran, "Numerical analysis of laser paint removal from various substrates," in *ROMOPTO 2012: Tenth Conference on Optics: Micro- to Nanophotonics III*, 2013, vol. 8882. doi: 10.1117/12.2032660.
[28] Y. Lu, L. Yang, M. Wang, and Y. Wang, "Simulation of nanosecond laser cleaning the paint based on the thermal stress," *Optik*, 2020, doi: 10.1016/j.ijleo.2020.165589.
[29] S. Akhtar, O. O. Kardas, O. Keles, and B. S. Yilbas, "Laser cutting of rectangular geometry into aluminum alloy: Effect of cut sizes on thermal stress field," *Optics and Lasers in Engineering*, vol. 61, 2014, doi: 10.1016/j.optlaseng.2014.04.016.
[30] O. O. Kardas, O. Keles, S. Akhtar, and B. S. Yilbas, "Laser cutting of rectangular geometry in 2024 aluminum alloy: Thermal stress analysis," *Optics and Laser Technology*, vol. 64, 2014, doi: 10.1016/j.optlastec.2014.05.029.
[31] D. Lee, R. Patwa, H. Herfurth, and J. Mazumder, "Computational and experimental studies of laser cutting of the current collectors for lithium-ion batteries," *Journal of Power Sources*, vol. 210, pp. 327–338, Jul. 2012, doi: 10.1016/j.jpowsour.2012.03.030.

[32] D. Lee, R. Patwa, H. Herfurth, and J. Mazumder, “High speed remote laser cutting of electrodes for lithium-ion batteries: Anode,” *Journal of Power Sources*, vol. 240, pp. 368–380, 2013, doi: 10.1016/j.jpowsour.2012.10.096.
[33] D. Lee and J. Mazumder, “Numerical studies of laser cutting of an anode for lithium-ion batteries,” in *ICALEO 2012 - 31st International Congress on Applications of Lasers and Electro-Optics*, 2012, pp. 1252–1260. doi: 10.2351/1.5062418.
[34] D. Lee, R. Patwa, H. Herfurth, and J. Mazumder, “High speed remote laser cutting of electrodes for lithium-ion batteries: Anode,” *Journal of Power Sources*, vol. 240, 2013, doi: 10.1016/j.jpowsour.2012.10.096.
[35] Y. Wang, Y. Chen, Y. Zhang, H. Chen, and S. Yu, “Generalised Hermite-Gaussian beams and mode transformations,” *Journal of Optics (United Kingdom)*, vol. 18, no. 5, 2016, doi: 10.1088/2040-8978/18/5/055001.
[36] F. Caiazzo and V. Alfieri, “Simulation of laser heating of aluminum and model validation via two-color pyrometer and shape assessment,” *Materials*, vol. 11, no. 9, 2018, doi: 10.3390/ma11091506.
[37] F. Caiazzo and V. Alfieri, “Simulation of laser-assisted directed energy deposition of aluminum powder: Prediction of geometry and temperature evolution,” *Materials*, vol. 12, no. 13, 2019, doi: 10.3390/ma12132100.
[38] V. Nasrollahi, P. Penchev, A. Batal, H. Le, S. Dimov, and K. Kim, “Laser drilling with a top-hat beam of micro-scale high aspect ratio holes in silicon nitride,” *Journal of Materials Processing Technology*, vol. 281, 2020, doi: 10.1016/j.jmatprotec.2020.116636.
[39] M. Srećković, Z. Karastojković, M. Janićijević, and Z. Stević, “Laser beam drilling and cutting of PMMA,” *Mining and Metallurgy Engineering Bor*, no. 3–4, 2017, doi: 10.5937/mmeb1704123s.
[40] I. Sindhu and R. A. Rahman, “Formation of microgrooves on glass and PMMA using low power CO2 laser,” *Journal of Optoelectronics and Advanced Materials*, vol. 14, no. 11–12, 2012.
[41] P. Joyce, J. Radice, A. Tresansky, and J. Watkins, “A COMSOL Model of Damage Evolution Due to High Energy Laser Irradiation of Partially Absorptive Materials,” *COMSOL Conference*, 2012.
[42] H. Karbasi, “Computer simulation of laser material removal: Measuring the depth of penetration in laser engraving,” 2008. doi: 10.2351/1.5061423.
[43] H. Karbasi, “COMSOL Assisted Simulation of Laser Engraving,” *COMSOL Conference*, 2010.
[44] J. Luo, S. Hou, J. Xu, W. Yang, and Y. Zhao, “Numerical modeling on carbon fiber composite material in Gaussian beam laser based on ANSYS,” 2014. doi: 10.1117/12.2054250.
[45] J. Zhang and L. Long, “Finite element simulation for laser ablation of carbon fiber epoxy composite,” 2011. doi: 10.4028/www.scientific.net/AMM.66-68.715.
[46] C. W. Wu, X. Q. Wu, and C. G. Huang, “Ablation behaviors of carbon reinforced polymer composites by laser of different operation modes,” *Optics and Laser Technology*, 2015, doi: 10.1016/j.optlastec.2015.04.008.
[47] Y. Wang, O. I. Zhupanska, and C. L. Pasiliao, “Verification of a manual mesh moving finite element analysis procedure for modeling ablation in laminated composite materials,” 2017. doi: 10.1115/IMECE2017-70623.
[48] Y. Wang and C. L. Pasiliao, “Modeling ablation of laminated composites: A novel manual mesh moving finite element analysis procedure with ABAQUS,” *International Journal of Heat and Mass Transfer*, 2018, doi: 10.1016/j.ijheatmasstransfer.2017.09.038.
[49] F. J. Prinsloo, S. P. van Heerden, E. Ronander, and L. R. Botha, “Efficient TEA CO 2 -laser-based coating removal system,” 2006. doi: 10.1117/12.739109.
[50] A. Tsunemi *et al.*, “Complete removal of paint from metal surface by ablation with a TEA CO2 laser,” *Applied Physics A: Materials Science and Processing*, 1996, doi: 10.1007/s003390050413.
[51] P. Nan, Z. Shen, B. Han, and X. Ni, “The influences of laminated structure on the ablation characteristics of carbon fiber composites under CW laser irradiation,” *Optics and Laser Technology*, 2019, doi: 10.1016/j.optlastec.2019.03.015.
[52] G. Guerrero-Vaca, Ó. Rodríguez-Alabanda, P. E. Romero, C. Soriano, E. Molero, and J. Lambarri, “Stripping of PFA fluoropolymer coatings using a Nd:YAG laser (Q-Switch) and an Yb fiber laser (CW),” *Polymers*, 2019, doi: 10.3390/polym11111738.
[53] P. B. Zhang, Y. Qin, J. J. Zhao, and B. Wen, “Two-dimensional numerical simulation of laser-

ablation of aluminum material by nanosecond laser pulse," *Wuli Xuebao/Acta Physica Sinica*, 2010, doi: 10.7498/aps.59.7120.

[54] T. E. Itina, M. E. Povarnitsyn, and K. v. Khishchenko, "Modeling of laser ablation induced by nanosecond and femtosecond laser pulses," in *Laser Ablation: Effects and Applications*, 2011.

[55] W. S. O. Rodden, S. S. Kudesia, D. P. Hand, and J. D. C. Jones, "A comprehensive study of the long pulse Nd:YAG laser drilling of multi-layer carbon fibre composites," *Optics Communications*, 2002, doi: 10.1016/S0030-4018(02)01807-2.

[56] L. Gao *et al.*, "Numerical Simulation and Surface Morphology of Laser-Cleaned Aluminum Alloy Paint Layer," *Zhongguo Jiguang/Chinese Journal of Lasers*, 2019, doi: 10.3788/CJL201946.0502002.

[57] M. Darif, N. Semmar, and F. O. Cedex, "Numerical Simulation of Si Nanosecond Laser Annealing by COMSOL Multiphysics," *... of the COMSOL Conference ...*, 2008.

[58] W. J. Keller *et al.*, "Physics of picosecond pulse laser ablation," *Journal of Applied Physics*, 2019, doi: 10.1063/1.5080628.

[59] L. Ke, H. Zhu, W. Lei, and Z. Cheng, "Laser cleaning of rust on ship steel using TEA CO 2 pulsed laser," 2009. doi: 10.1117/12.846775.

[60] M. Sundar, P. T. Mativenga, L. Li, and P. L. Crouse, "Laser removal of TiN from coated carbide substrate," *International Journal of Advanced Manufacturing Technology*, 2009, doi: 10.1007/s00170-009-2059-y.

[61] S. Marimuthu *et al.*, "Laser stripping of TiAlN coating to facilitate reuse of cutting tools," 2011. doi: 10.1177/0954405411414313.

[62] F. Li, X. Chen, W. Lin, H. Pan, X. Jin, and X. Hua, "Nanosecond laser ablation of Al-Si coating on boron steel," *Surface and Coatings Technology*, 2017, doi: 10.1016/j.surfcoat.2017.03.038.

[63] S. G. Pantelakis, T. B. Kermanidis, and G. N. Haidemenopoulos, "Mechanical behavior of 2024 Al alloy specimen subjected to paint stripping by laser radiation and plasma etching," *Theoretical and Applied Fracture Mechanics*, 1996, doi: 10.1016/0167-8442(96)00016-X.

[64] M. Kumar *et al.*, "Epoxy-paint stripping using TEA CO 2 laser: Determination of threshold fluence and the process parameters," *Optics and Laser Technology*, 2013, doi: 10.1016/j.optlastec.2012.04.021.

[65] F. J. Prinsloo, S. P. van Heerden, E. Ronander, and L. R. Botha, "Efficient TEA CO 2 -laser-based coating removal system," in *XVI International Symposium on Gas Flow, Chemical Lasers, and High-Power Lasers*, Sep. 2006, vol. 6346, p. 63462Q. doi: 10.1117/12.739109.

[66] A. Tsunemi, A. Endo, and D. Ichishima, "titlePaint removal from aluminum and composite substrate of aircraft by laser ablation using TEA COformulainfroman2/roman/inf/formulalasers/title," in *High-Power Laser Ablation*, Sep. 1998, vol. 3343, pp. 1018–1022. doi: 10.1117/12.321539.

[67] C. W. Wu, X. Q. Wu, and C. G. Huang, "Ablation behaviors of carbon reinforced polymer composites by laser of different operation modes," *Optics and Laser Technology*, vol. 73, pp. 23–28, Oct. 2015, doi: 10.1016/j.optlastec.2015.04.008.

[68] M. S. F. Lima, J. M. S. Sakamoto, J. G. A. Simoes, and R. Riva, "Laser processing of carbon fiber reinforced polymer composite for optical fiber guidelines," in *Physics Procedia*, 2013, vol. 41, pp. 572–580. doi: 10.1016/j.phpro.2013.03.118.

[69] W. S. O. Rodden, S. S. Kudesia, D. P. Hand, and J. D. C. Jones, "A comprehensive study of the long pulse Nd:YAG laser drilling of multi-layer carbon fibre composites," *Optics Communications*, vol. 210, no. 3–6, pp. 319–328, Sep. 2002, doi: 10.1016/S0030-4018(02)01807-2.

[70] Y. K. Madhukar, S. Mullick, D. K. Shukla, S. Kumar, and A. K. Nath, "Effect of laser operating mode in paint removal with a fiber laser," *Applied Surface Science*, vol. 264, pp. 892–901, Jan. 2013, doi: 10.1016/j.apsusc.2012.10.193.

[71] J. Mathew, G. L. Goswami, N. Ramakrishnan, and N. K. Naik, "Parametric studies on pulsed Nd:YAG laser cutting of carbon fibre reinforced plastic composites," *Journal of Materials Processing Technology*, vol. 89–90, pp. 198–203, May 1999, doi: 10.1016/S0924-0136(99)00011-4.

[72] "Ablation behaviors of carbon reinforced polymer composites by laser of different operation modes - ScienceDirect." [Online]. Available: https://www.sciencedirect.com/science/article/pii/S0030399215001024

[73] T. Heiderscheit, N. Shen, Q. Wang, A. Samanta, B. Wu, and H. Ding, "Keyhole cutting of carbon fiber reinforced polymer using a long-duration nanosecond pulse laser," *Optics and Lasers in Engineering*, vol. 120, pp. 101–109, Sep. 2019, doi:

10.1016/j.optlaseng.2019.03.009.
[74] M. Fujita *et al.*, “Wavelength and pulsewidth dependences of laser processing of CFRP,” in *Physics Procedia*, 2016, vol. 83, pp. 1031–1036. doi: 10.1016/j.phpro.2016.08.108.
[75] C. A. Griffis, R. A. Masumura, and C. I. Chang, “Thermal Response of Graphite Epoxy Composite Subjected to Rapid Heating,” *Journal of Composite Materials*, vol. 15, no. 5, pp. 427–442, 1981, doi: 10.1177/002199838101500503.
[76] J. P. Fanucci, “Thermal Response of Radiantly Heated Kevlar and Graphite/Epoxy Composites,” *Journal of Composite Materials*, vol. 21, no. 2, pp. 129–139, 1987, doi: 10.1177/002199838702100204.
[77] R. Negarestani *et al.*, “Numerical simulation of laser machining of carbon-fibre-reinforced composites,” *Proceedings of the Institution of Mechanical Engineers, Part B: Journal of Engineering Manufacture*, vol. 224, no. 7, pp. 1017–1027, Jul. 2010, doi: 10.1243/09544054jem1662.
[78] K. Liu and E. Garmire, “Paint removal using lasers,” *Applied Optics*, vol. 34, no. 21, p. 4409, Jul. 1995, doi: 10.1364/AO.34.004409.
[79] X. Li, T. Huang, A. W. Chong, R. Zhou, Y. S. Choo, and M. Hong, “Laser cleaning of steel structure surface for paint removal and repaint adhesion,” *Opto-Electronic Engineering, Vol.44, Issue 03, pp. 340*, vol. 44, no. 03, pp. 340–344, Mar. 2017, doi: 10.3969/j.issn.1003-501x.2017.03.009.
[80] A. Slocombe and L. Li, “Laser ablation machining of metal/polymer composite materials,” *Applied Surface Science*, vol. 154–155, pp. 617–621, Feb. 2000, doi: 10.1016/S0169-4332(99)00391-8.
[81] M. A. Belcher, C. J. Wohl, J. W. Hopkins, and J. W. Connell, “Laser Surface Preparation and Bonding of Aerospace Structural Composites,” May 2010, [Online]. Available: https://ntrs.nasa.gov/search.jsp?R=20100021129
[82] P. W. Kopf, J. Cheney, and J. Martin, “Paint Removal from Composites and Protective Coating Development,” 1991. [Online]. Available: https://apps.dtic.mil/docs/citations/ADA249238
[83] A. Tsunemi *et al.*, “Complete removal of paint from metal surface by ablation with a TEA CO2 laser,” *Applied Physics A Materials Science & Processing*, vol. 63, no. 5, pp. 435–439, Nov. 1996, doi: 10.1007/BF01571670.
[84] G. X. Chen, T. J. Kwee, K. P. Tan, Y. S. Choo, and M. H. Hong, “Laser cleaning of steel for paint removal,” *Applied Physics A*, vol. 101, no. 2, pp. 249–253, Nov. 2010, doi: 10.1007/s00339-010-5811-0.

[3]–[84]